RSC Advances

COMMUNICATION

Acid/redox dual-activated liposomes for tumor-targeted drug delivery and enhanced therapeutic efficacy†

Cite this: *RSC Adv.*, 2015, **5**, 67803

Received 10th April 2015
Accepted 31st July 2015

DOI: 10.1039/c5ra06445g

www.rsc.org/advances

Xuefan Xu,[a] Lei Zhang,[a] Assogba G. Assanhou,[ab] Lu Wang,[a] Yidi Zhang,[a] Wenyuan Li,[c] Lingjing Xue,[a] Ran Mo*[a] and Can Zhang*[a]

Acid/redox dual-activated liposomes consisting of a synthetic functional lipid were developed to overcome the multiple barriers to the intravenous delivery of an anticancer drug from the injection site to the target site. The liposome exhibited tumor pH-promoted cellular uptake, endocytic pH-responsive endo-lysosomal escape and redox-triggered intracellular drug release, thereby yielding enhanced antitumor activity.

Great progress has been made in nanoparticle (NP)-based tumor-targeted drug delivery systems such as micelles,[1–3] nanogels,[4–6] and liposomes[7–10] in the last few decades. Drugs loaded in liposomes exhibit pharmacokinetic profiles of the vesicles until their release from the carriers at the target sites. In view of this, the anticancer efficacy of NPs depends on both the ability to reach the tumor tissue and the release rate of the encapsulated drug from the vector at the site of action to a great extent.[11,12] There are multiple obstacles required to be circumvented for anticancer drug to take effect, including transport from blood circulation to the tumor, permeation across the cell membrane into the tumor cell, migration from the endocytic vesicles to the cytoplasm and release from the NPs within the tumor cell.

The pH in the tumor microenvironment (pH 6.0–7.0) is lower than that in blood and normal tissues, and becomes more acidic (pH 5.0–6.0) in the endocytic vesicles.[13] In addition, glutathione (GSH), a thiol-containing tripeptide, shows extremely higher concentration (1–10 mM) inside cells than outside (2–20 μM), which provides an ideal signal for programmed intracellular drug release. More importantly, the tumor tissue has been demonstrated to be more reducing with a GSH level 4-fold at least higher than that in the normal cells, which can be used for tumor-targeted drug delivery.[14,15] Although a variety of drug carriers have been designed by exploiting such remarkable pH or reductive gradient for tackling the challenges in NP-based antitumor drug delivery, most reports have only focused on surmounting one or two obstacles, such as increasing the tumor cellular uptake by tumor acid-responsive dePEGylation[16,17] or charge conversion,[18,19] or enhancing the endo-lysosomal escape responding to the endocytic pH,[20–22] or promoting the intracellular drug release modulated by the cytoplasmic GSH.[23–25] In our previous work, a multistage pH-responsive liposome has been developed to overcome the multiple barriers in the whole delivery process.[21] However, this formulation was limited by relatively slow drug release in the cells.

Herein, we report an acid/redox dual-responsive liposome (HH-SS-L) for enhanced antitumor efficacy, which was developed by integrating the capability of conquering the barriers from the blood to the target site and that of controlling the intracellular drug release in one nanocarrier (Fig. 1). HH-SS-L are fabricated by soy phosphatidylcholine (SPC), 1,2-dioleoyl-*sn-glycero*-3-phosphoethanolamine (DOPE), and a synthetic functional lipid, 2-[2-(2-carboxylcyclohexylformamido)-3,12-dioxy-1-(1*H*-imidazolyl-4)-7,8-dithio-4,11-diazapentadecylamide]-glutaric acid ditetradecanol-diester (HH-SS-E2C_{14}). HH-SS-E2C_{14} contains one amino acid group (histidine) and one acid-cleavable group (hexahydrobenzoic (HHB) amide) as a hydrophilic block, and two tetradecyl alkane chains as a hydrophobic block. A disulfide bond is incorporated as a redox-sensitive linkage between the two blocks. After intravenous administration, the surface charge of HH-SS-L in blood circulation is strongly negative. Once arriving at the tumor extracellular matrix *via* the enhanced permeability and retention (EPR) effect, the surface charge of the liposome changes from negative to positive for increased tumor cellular uptake owing to electrostatic adsorption with the negatively charged cell

[a]*State Key Laboratory of Natural Medicines, Jiangsu Key Laboratory of Drug Discovery for Metabolic Diseases, Center of Drug Discovery, China Pharmaceutical University, Nanjing 210009, China. E-mail: rmo@cpu.edu.cn; zhangcan@cpu.edu.cn*

[b]*UFR Pharmacie, Faculté des Sciences de la Santé, Université d'Abomey-calavi, 01 BP 188, Cotonou, Benin*

[c]*Faculty of Pharmacy and Pharmaceutical Sciences, Monash University, Parkville, VIC 3052, Australia*

† Electronic supplementary information (ESI) available: Synthesis of HH-SS-E2C_{14}, preparation and characterization of DOX/HH-SS-L, *in vitro* cell studies and *in vivo* animal investigations. See DOI: 10.1039/c5ra06445g

membrane. After endocytosis, the protonation of the imidazole group in HH-SS-E2C_{14} promotes proton influx into the endocytic vesicles, endo-lysosomes, followed by the osmotic pressure increase, endo-lysosomal rupture and thereby endo-lysosomal escape into cytoplasm. Meanwhile, the degradation of the HHB amide results in more positive charge of liposome in the endo-lysosomes, which further advances the endo-lysosomal escape. When migrated into the cytoplasm, the liposome disrupts caused by the intracellular GSH-mediated cleavage of HH-SS-E2C_{14}, which leads to a prompt and rapid release of doxorubicin hydrochloride (DOX), a model small-molecule chemotherapeutic drug for inducing cytotoxicity.

To validate this assumption, HH-SS-E2C_{14} and control lipids, including HH-E2C_{14} (without the disulfide bond), H-SS-E2C_{14} (without the HHB amide) and H-E2C_{14} (without the disulfide bond and HHB amide), were synthesized and characterized (Schemes S1 and 2†). DOX-loaded HH-SS-L (DOX/HH-SS-L) were prepared with a particle size of 131 nm using the ammonium sulfate gradient method, which had an entrapment efficiency of 96% and a drug-loading capacity of 3% (Table S1†). Compared with the cationic DOX/H-SS-L, DOX/HH-SS-L showed a negative surface charge due to the deprotonation of carboxylic acid in the HHB amide (Table S1†).

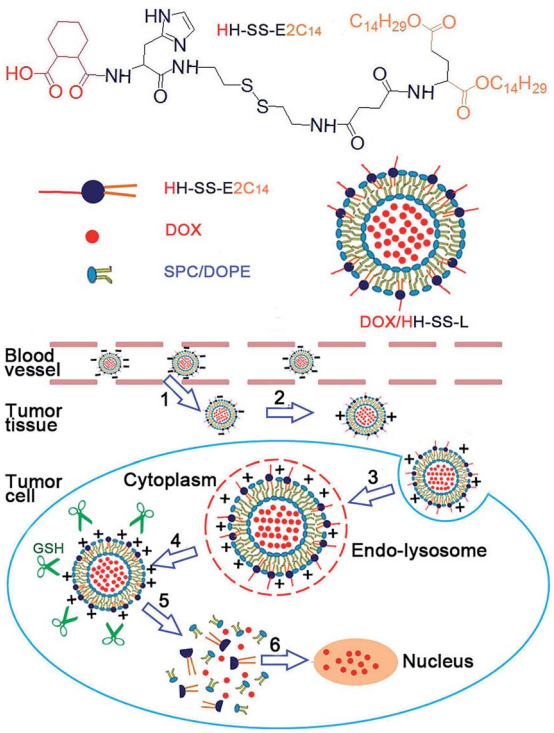

Fig. 1 Schematic illustration of DOX/HH-SS-L consisting of SPC, DOPE and HH-SS-E2C_{14} for tumor-targeted drug delivery. SPC: soy phosphatidylcholine; DOPE: 1,2-dioleoyl-*sn*-*glycero*-3-phosphoethanolamine; HH-SS-E2C_{14}: the synthetic functional lipid (Scheme S1†). (1) Accumulation of liposome at the tumor site; (2) tumor pH-activated charge conversion; (3) endocytosis; (4) endo-lysosomal escape; (5) GSH-triggered intracellular DOX release; (6) accumulation of the released DOX into the nucleus for cytotoxicity.

To evaluate the acid-activated charge conversion property of HH-SS-L, the change in the zeta potential was monitored (Fig. S1†) in the buffer solutions or the fetal bovine serum (FBS) supplemented cell culture media with different pH. The surface charge of HH-SS-L underwent conversion in response to the pH variation, which was negative at pH 7.4 (physiological pH) while positive at pH 6.5 (a typical tumor pH) and highly positive at pH 4.5 (a typical lysosomal pH). The similar tendency was determined in HH-L. In sharp contrast, the conventional liposome, SPC-L, presented no pH-responsiveness, which had a constant negative charge regardless of pH. No apparent increase of the average particle sizes of liposomes was observed (Fig. S2†), indicating no aggregation occurred under different pH conditions. In addition, the acid-sensitive degradation of the HHB amide, accompanied by the shedding of the carboxylic acid and the exposure of the amino group, resulted in a much higher positive charge of both HH-SS-L and HH-L after incubation under acidic conditions for a longer time (Fig. S3 and S4†). The hydrolysis kinetics of the HHB amide was examined using the fluorescamine method.[26,27] After 24 h of incubation, the degradation percentage was around 49% and 72% for HH-SS-L at pH 5.5 and at pH 4.5, respectively. By contrast, only about 11% and 20% of the HHB amide was hydrolyzed for HH-SS-L at pH 7.4 and pH 6.5, respectively (Fig. 2a). The same tendency with HH-SS-L happened to HH-L (Fig. S5†). These data suggested that the obtained HH-SS-L had the charge conversion capability in response to the environmental pH change. The more acidity caused the higher positive surface charge. Furthermore, the proton buffering capacity of HH-SS-L was estimated using the titration method (Fig. S6†). Both of HH-SS-L and HH-L composed of the histidine-containing lipid possessed a greater pH-buffering effect when the surrounding pH reduced from neutral to acid compared with SPC-L, which endued HH-SS-L and HH-L with the endo-lysosomal escape capability for efficient intracellular delivery.

To demonstrate the redox sensitivity of the disulfide-containing liposomes, the degradation of H-SS-2EC_{14} in H-SS-L was first investigated in the presence of GSH (Fig. 2b). The degradation percentage of H-SS-E2C_{14} had a positive correlation with the concentration of GSH. The cleaved percentage of H-SS-E2C_{14} was approximately 4%, 30% and 70% after incubation of H-SS-L with GSH at the concentration of 10 μM, 1 mM and 10 mM, respectively. These results indicated that H-SS-E2C_{14} could be rapidly degraded in the reductive intracellular milieu (1–10 mM GSH) rather than in the physiological environment (around 10 μM GSH), which might induce the instability of liposomes and thereby facilitate the fast release of DOX inside the cancer cells.

To further evaluate the redox-triggered DOX release from liposomes caused by the GSH-mediated degradation of disulfide-containing lipid, the release profile of DOX/HH-SS-L was determined in the presence of different concentrations of GSH using the dialysis method (Fig. 2c). The cumulative amount of DOX released from DOX/HH-SS-L was about 60% and 70% after incubation with 10 mM GSH at pH 7.4 and 5.5 for 4 h, respectively, which increased to over 80% after 8 h of incubation. However, DOX/HH-SS-L showed noticeably lower

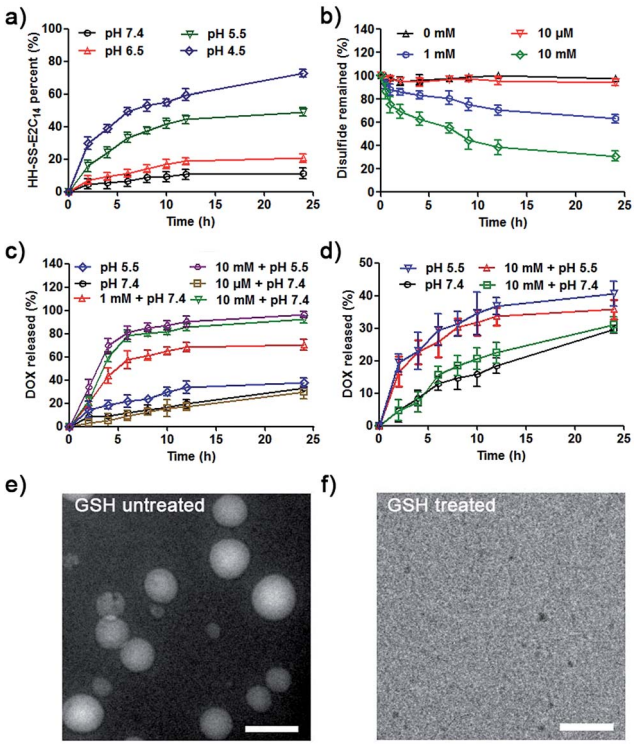

Fig. 2 (a) Degradation of the HHB amide in HH-SS-L at different pH values over time. (b) Degradation of H-SS-E2C$_{14}$ at different concentrations of GSH over time. (c and d) *In vitro* release profiles of DOX from DOX/HH-SS-L (c) and DOX/HH-L (d) under different conditions. (e and f) TEM images of DOX/HH-SS-L before (e) and after (f) treatment with 10 mM GSH for 24 h. Scale bars are 200 nm.

release rate of DOX in the presence of 10 μM GSH. Moreover, no significant difference in the release of DOX from either DOX/SPC-L (Fig. S7†) or DOX/HH-L (Fig. 2d) between 0 mM and 10 mM GSH at the same pH. Additionally, the transmission electronic microscope (TEM) examination further suggested that treatment with GSH resulted in the disruption of DOX/HH-SS-L. Compared with non-treatment (Fig. 2e), no spherical structure was observed after incubation with 10 mM GSH at 37 °C for 24 h (Fig. 2f). These data demonstrated that the cytoplasmic GSH could reduce the disulfide bridge in HH-SS-E2C$_{14}$, induce the liposomal instability and thus trigger the abundant DOX release within the cells.

Next, the acid-promoted cellular uptake of liposome was gauged on the human hepatic carcinoma (HepG2) cells (Fig. S8†). As expected, the cellular uptake of DOX at pH 6.5 was significantly higher than that at pH 7.4 for both DOX/HH-L and DOX/HH-SS-L, which suggested that the positive charge on the surface of DOX/HH-L or DOX/HH-SS-L in the slightly acidic tumor tissues contributed to the promoted internalization of liposomes.[28,29] In contrast, for DOX/SPC-L with a similar particle size, the uptake amount of DOX at pH 6.5 was comparable to that at pH 7.4, and lower than that of DOX/HH-L or DOX/HH-SS-L at pH 6.5, which further signified that the electrostatic interaction between liposome and cell played an important role in facilitating vanquishing the cellular barrier, cell membrane. Whereas, the clathrin-mediated endocytic pathway was a typical route, by which DOX/HH-SS-L was internalized into the cells (Fig. S9†),[30,31] implying that the endo-lysosomes became the subcellular barrier to the intracellular delivery.[32]

The endo-lysosomal escape behavior and intracellular release property of the liposomes were assessed using confocal laser scanning microscope (CLSM). Specifically, after incubation with the DOX-loaded liposomal preparations, the endo-lysosomes were selectively stained with LysoTracker Green shown as a green fluorescence, while the liposomes encapsulating DOX were observed as a red fluorescence. Co-localization between the DOX signal and the endo-lysosomal signal indicated the entrapment of liposome in the endo-lysosomes. As shown in Fig. 3 and S10,† a large number of yellow dots were evident in the merged images after addition of the DOX-loaded liposomes for 2 h, which implied that a large part of DOX were entrapped within the endo-lysosomal compartments following endocytosis. After a prolonged incubation, in DOX/SPC-L group, the DOX signal still remained highly overlaying with the endo-lysosomal signal and could not be observed in the nuclei, indicating that it was very difficult for the conventional DOX/SPC-L to escape from the endo-lysosomes. However, the DOX signal of DOX/HH-SS-L or DOX/HH-L showed a obviously great separation with the endo-lysosomal signal, which confirmed their superior endo-lysosomal escape capability of overthrowing the endocytic barrier due to the proton sponge effect of histidines and highly positive surface charge of DOX/HH-SS-L and DOX/HH-L.[20–22] In addition, compared with DOX/HH-L, DOX/HH-SS-L with the potency of intracellular GSH-triggered drug release showed a stronger effect on delivering DOX to its target site, nuclei. Higher fluorescence intensity of the DOX signal in the nuclei delivered by DOX/HH-SS-L was observed. It was verified that the disintegration of DOX/HH-SS-L in response to the intracellular GSH level generated a prompt and burst release of DOX, which efficiently overcome the final barrier, nanocarrier, to attain the therapeutic concentration of drug inside the cancer cells for enhanced anticancer activity.

The *in vitro* therapeutic efficacy of DOX/HH-SS-L was evaluated on HepG2 cells. The apoptosis-inducing effect of DOX/HH-SS-L was first determined using the Annexin V-FITC/PI staining, followed by the flow cytometric analysis (Fig. 4a). The total

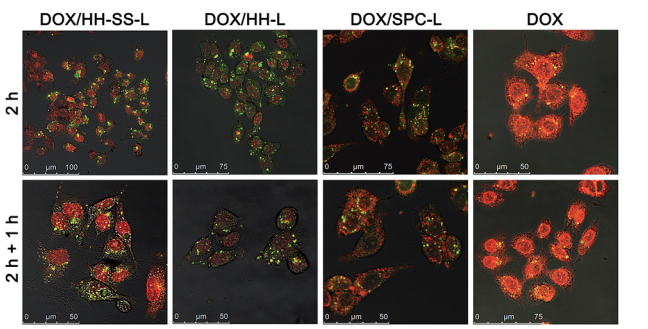

Fig. 3 CLSM images of HepG2 cells after incubation with DOX/SPC-L, DOX/HH-L, DOX/HH-SS-L and free DOX for different time. The late endosomes and lysosomes were stained with LysoTracker Green.

apoptotic ratio was 4% after the cells were treated with DOX/SPC-L, while increased to 9.5% when incubated with DOX/HH-L, which substantiated that the enhanced cellular uptake and endo-lysosomal escape had an apparent enhancement on inducing cell apoptosis. Of note, although there was no significant difference in the cellular uptake between DOX/HH-SS-L and DOX/HH-L, DOX/HH-SS-L presented a significantly stronger apoptosis-inducing capacity compared with DOX/HH-L, which had the total apoptotic ratio of 18.1%, nearly 2-fold that of DOX/HH-L, substantiating that the fast intracellular drug release contributed greatly to the elevated induction of apoptosis in the cancer cells. In addition, the cytotoxicity of DOX/HH-SS-L toward HepG2 was evaluated using the MTT method (Fig. S11† and 4b). DOX/HH-SS-L exhibited a higher cytotoxicity against HepG2 cells than either DOX/SPC-L or DOX/HH-L. The half maximal inhibitory concentration (IC_{50}) of DOX/HH-SS-L was about 1.91 μg mL^{-1} for 48 h (Fig. S11†). As time extended to 72 h, the IC_{50} reduced to approximately 1.14 μg mL^{-1} (Fig. 4b), which was nearly 0.36-fold and 0.22-fold that of DOX/HH-L (roughly 3.14 μg mL^{-1}) and DOX/SPC-L (around 5.10 μg mL^{-1}), respectively. The bare liposome did not present any cytotoxicity at all the tested concentrations (Fig. S12†).

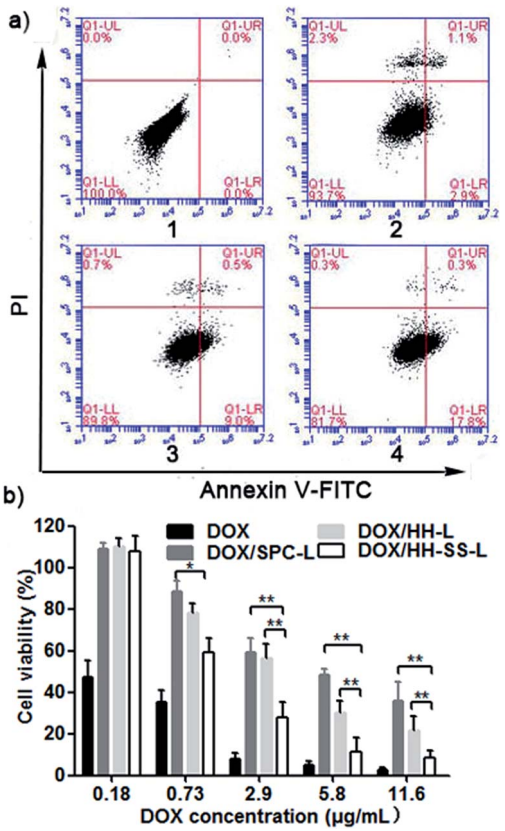

Fig. 4 (a) Flow cytometric analysis of apoptosis induced by different DOX formulations using the Annexin V-FITC/PI staining. (1) Control; (2) DOX/SPC-L; (3) DOX/HH-L; (4) DOX/HH-SS-L. (b) *In vitro* cytotoxicity of the free DOX, DOX/SPC-L, DOX/HH-L and DOX/HH-SS-L against HepG2 cells for 72 h. *$P < 0.05$, **$P < 0.01$.

Next, we compared the tumor-targeting ability of HH-SS-L with that of HH-L and SPC-L *in vivo*. The liposomes were labeled with the lipophilic fluorescent dye DiR. After intravenous injection into the xenograft Heps tumor-bearing mice, the DiR signal was monitored using the *in vivo* imaging (Fig. 5a). At just 1 h post-injection, the DiR signal of DiR/HH-SS-L was observed at the tumor site, increased at 12 h, and maintained up to 24 h. HH-SS-L displayed greater tumor targetability than HH-L and SPC-L. To further investigate the enhancement on the DOX accumulation in the tumor by HH-SS-L, the amount of DOX was quantified in the plasma and different tissues including heart, liver, spleen, lung, kidney and tumor after intravenous injection of different DOX formulations (Fig. 5b and S13†). Compared with the free DOX solution, different DOX liposomes showed prolonged blood circulation and enhanced tumor accumulation of DOX. Note that the accumulation of DOX in the heart delivered by the liposomes was extremely lower than that delivered by the DOX solution, which indicated that the liposomal formulations could optimize the biodistribution property of DOX and therefore reduce the cardiotoxicity of DOX. The majority of the liposomes accumulated in the liver and spleen, which suggested that the reticuloendothelial system (RES) uptake of liposomes played an important part in the elimination of liposomes after systemic administration. No significant difference in the cellular uptake among three different liposomes by the murine macrophages (RAW264.7) implied no specific RES uptake of these liposomes (Fig. S14†), which was consistent with the results of DOX distribution of different liposomes in the liver and spleen. By comparison, the accumulation and retention of DOX/HH-SS-L in the tumor was much higher than that of DOX/SPC-L, while

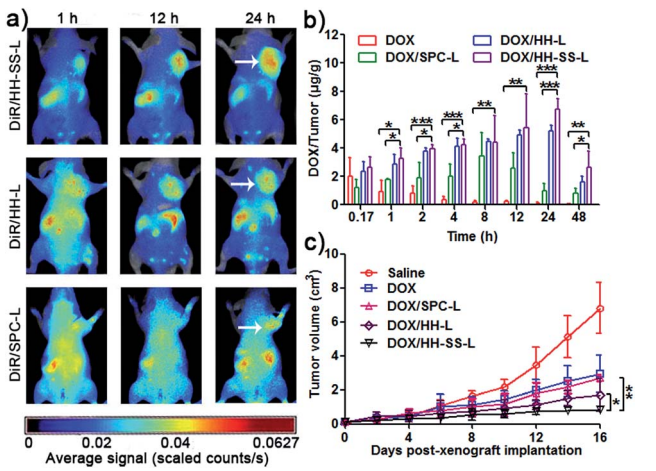

Fig. 5 (a) *In vivo* fluorescence images of the xenograft Heps tumor-bearing mice after intravenous injection of DiR/SPC-L, DiR/HH-L and DiR/HH-SS-L. The white arrows indicate the tumor regions. (b) Quantification on the accumulation of DOX in the tumor of the tumor-bearing mice after intravenous injection of different DOX formulations at a DOX dose of 5 mg kg^{-1}. DOX/tumor is the ratio of the DOX amount in the tumor (μg) to the tumor weight (g). *$P < 0.05$, **$P < 0.01$, ***$P < 0.001$. (c) Change in the tumor size of the tumor-bearing mice after treatment with saline, the free DOX, DOX/SPC-L, DOX/HH-L and DOX/HH-SS-L at a DOX dose of 5 mg kg^{-1}. *$P < 0.05$, **$P < 0.01$.

no significant difference in the tumor targetability between DOX/HH-SS-L and DOX/HH-L was found, which demonstrated that the tumor pH-activated charge conversion capacity of DOX/HH-SS-L and DOX/HH-L had crucial effect on increasing the DOX concentration at the tumor site. By comparing the results obtained from the quantification of DOX with that from the qualitative/semi-quantitative fluorescent imaging, we found that more DiR signal of DiR/HH-SS-L was determined in the liver and spleen at 24 h post-injection, compared with DiR/SPC-L or DiR/HH-L (Fig. S15 and S16†), which was not in agreement with the DOX quantification results showing no significant difference in both liver and spleen distribution of DOX among three liposomes (Fig. S13c and d†). According to the macrophage uptake study, it was suggested that the quantitative analysis is more accurate and straightforward than the qualitative/semi-quantitative fluorescent imaging technique for the biodistribution study, which confirmed that no remarkable difference in the macrophage uptake and the DOX accumulation in the liver and spleen among these studied liposomes.

The *in vivo* antitumor efficacy of DOX/HH-SS-L was assessed on the Heps tumor-bearing mice. As shown in Fig. 5c, different DOX formulations presented inhibiting effect on tumor growth compared with saline as a negative control. DOX/HH-L manifested stronger effect than the DOX solution and DOX/SPC-L, which was mainly attributed to the improved tumor targeting and intracellular delivery of DOX by HH-L. Furthermore, compared with DOX/HH-L, DOX/HH-SS-L exhibited significant enhanced therapeutic efficacy, suggesting that efficient intracellular DOX release could further dramatically reinforce the antitumor activity. Moreover, a comprehensive elimination of the cancer cells was observed in the tumor tissue after the DOX/HH-SS-L treatment by the histological analysis using the hematoxylin and eosin staining (Fig. S17†) and no evident change in the body weight of the tumor-bearing mice during the treatment with DOX/HH-SS-L compared with saline (Fig. S18†).

Conclusion

In this study, we developed a new acid/redox dual-activated liposome for anticancer drug delivery. Acid-sensitivity brought about the enhanced cellular uptake and the proton sponge effect for successively overcoming the cellular and intracellular barriers. Redox-triggered drug release property provided a great potential to conquer the nanocarrier-derived barrier for promoted therapeutic efficacy. This work aiming to overpower all the barriers during the NP-based drug delivery process opens up a considerable prospect for enhanced antitumor efficiency.

Acknowledgements

This work was supported by the National Natural Science Foundation of China (81273468, 81473153), National Basic Research Program of China (2015CB755500), Natural Science Foundation of Jiangsu Province of China (BK20140672), Fundamental Research Funds for the Central Universities of China, State Key Laboratory of Natural Medicines at China Pharmaceutical University (CPU) (SKLNMZZCX201401) and 111 Project from the Ministry of Education of China and the State Administration of Foreign Expert Affairs of China (No. 111-2-07). This work was also supported by the Jiangsu Specially-Appointed Professors Program, the CPU High-Level Talent Program and the start-up package from CPU to R.M.

Notes and references

1 R. Mo, X. Jin, N. Li, C. Ju, M. Sun, C. Zhang and Q. Ping, *Biomaterials*, 2011, **32**, 4609.
2 P. Laskar, B. Saha, S. K. Ghosh and J. Dey, *RSC Adv.*, 2015, **5**, 16265.
3 H. C. Yen, H. Cabral, P. Mi, K. Toh, Y. Matsumoto, X. Liu, H. Koori, A. Kim, K. Miyazaki, Y. Miura, N. Nishiyama and K. Kataoka, *ACS Nano*, 2014, **8**, 11591.
4 C. Ju, R. Mo, J. Xue, L. Zhang, Z. Zhao, L. Xue, Q. Ping and C. Zhang, *Angew. Chem., Int. Ed.*, 2014, **53**, 6253.
5 R. Mo, T. Jiang, R. DiSanto, W. Tai and Z. Gu, *Nat. Commun.*, 2014, **5**, 3364.
6 Y. Lee, T. Ishii, H. Cabral, H. J. Kim, J. H. Seo, N. Nishiyama, H. Oshima, K. Osada and K. Kataoka, *Angew. Chem., Int. Ed.*, 2009, **48**, 5309.
7 R. Mo, T. Jiang and Z. Gu, *Angew. Chem., Int. Ed.*, 2014, **53**, 5815.
8 T. Jiang, R. Mo, A. Bellotti, J. Zhou and Z. Gu, *Adv. Funct. Mater.*, 2014, **24**, 2258.
9 E. Crucianelli, P. Bruni, A. Frontini, L. Massaccesi, M. Pisani, A. Smorlesi and G. Mobbili, *RSC Adv.*, 2014, **4**, 58204.
10 Y. Wang, L. Zhang, S. Guo, A. Hatefi and L. Huang, *J. Controlled Release*, 2013, **172**, 179.
11 D. Peer, J. M. Karp, S. Hong, O. C. Farokhzad, R. Margalit and R. Langer, *Nat. Nanotechnol.*, 2007, **2**, 751.
12 Z. Ge and S. Liu, *Chem. Soc. Rev.*, 2013, **42**, 7289.
13 S. Simoes, *Adv. Drug Delivery Rev.*, 2004, **56**, 947.
14 G. Saito, J. A. Swanson and K. D. Lee, *Adv. Drug Delivery Rev.*, 2003, **55**, 199.
15 P. Kuppusamy, H. Li, G. Ilangovan, A. J. Cardounel, J. L. Zweier, K. Yamada, M. C. Krishna and J. B. Mitchell, *Cancer Res.*, 2002, **62**, 307.
16 E. Koren, A. Apte, A. Jani and V. P. Torchilin, *J. Controlled Release*, 2012, **160**, 264.
17 X. Yang, J. Du, S. Dou, C. Mao, H. Long and J. Wang, *ACS Nano*, 2012, **6**, 771.
18 Y. Lee, K. Miyata, M. Oba, T. Ishii, S. Fukushima, M. Han, H. Koyama, N. Nishiyama and K. Kataoka, *Angew. Chem., Int. Ed.*, 2008, **47**, 5163.
19 J. Z. Du, T. M. Sun, W. J. Song, J. Wu and J. Wang, *Angew. Chem., Int. Ed.*, 2010, **49**, 3621.
20 T. Jiang, Z. Zhang, Y. Zhang, H. Lv, J. Zhou, C. Li, L. Hou and Q. Zhang, *Biomaterials*, 2012, **33**, 9246.
21 R. Mo, Q. Sun, J. Xue, N. Li, W. Li, C. Zhang and Q. Ping, *Adv. Mater.*, 2012, **24**, 3705.
22 K. Shigeta, S. Kawakami, Y. Higuchi, T. Okuda, H. Yagi, F. Yamashita and M. Hashida, *J. Controlled Release*, 2007, **118**, 262.

23 G. Gasparini, E. Bang, G. Molinard, D. V. Tulumello, S. Ward, S. O. Kelley, A. Roux, N. Sakai and S. Matile, *J. Am. Chem. Soc.*, 2014, **136**, 6069.
24 S. Lim, K. Hong, D. Kim, H. Kwon and H. Kim, *J. Am. Chem. Soc.*, 2014, **136**, 7018.
25 Y. Lu, R. Mo, W. Tai, W. Sun, D. B. Pacardo, C. Qian, Q. Shen, F. S. Ligler and Z. Gu, *Chem. Commun.*, 2014, **50**, 15105.
26 J. J. Morris and M. I. Page, *J. Chem. Soc., Chem. Commun.*, 1978, 591.
27 P. Xu, E. A. van Kirk, Y. Zhan, W. J. Murdoch, M. Radosz and Y. Shen, *Angew. Chem., Int. Ed.*, 2007, **46**, 4999.
28 W. Chen, K. Achazi, B. Schade and R. Haag, *J. Controlled Release*, 2015, **205**, 15.
29 Y. Obata, S. Tajima and S. Takeoka, *J. Controlled Release*, 2010, **142**, 267.
30 J. E. Heuser and R. G. W. Anderson, *J. Cell Biol.*, 1989, **108**, 389.
31 M. G. Qaddoumi, H. J. Gukasyan, J. Davda, V. Labhasetwar, K. J. Kim and V. H. L. Lee, *Mol. Vision*, 2003, **9**, 559.
32 F. M. Brodsky, C. Y. Chen, C. Knuehl, M. C. Towler and D. E. Wakeham, *Annu. Rev. Cell Dev. Biol.*, 2001, **17**, 517.

